Two–dimensional angular light–scattering in aqueous NaCl single aerosol particles during deliquescence and efflorescence

Christian Braun and Ulrich K. Krieger

Laboratorium für Atmosphärenphysik (LAPETH), Hönggerberg HPP, 8093 Zürich, Switzerland

braun@atmos.umnw.ethz.ch

krieger@atmos.umnw.ethz.ch

Abstract: We present a new method to analyze two–dimensional angular light–scattering patterns of single aerosol particles by image processing. A pattern distortion parameter can be calculated to determine the solid–to–liquid partitioning in micron sized composite particles similar to using temporal light–scattering intensity fluctuations. We use the scattering patterns during deliquescence of a NaCl crystal to prove the feasibility of the method. In addition we show that even fast processes like the efflorescence from a supersaturated solution droplet can be analyzed where temporal fluctuation analysis fails. We find that efflorescence cannot be described as a time reversed deliquescence. There is indication that during efflorescence a solid shell grows at the surface of the liquid droplet which finally collapses due to mechanical stress.

© 2001 Optical Society of America

OCIS codes: 010.1110 Aerosols; 100.2000 Digital image processing; 290.5820 Scattering measurements; 290.5850 Scattering, particles

References and links

1. S. Holler, J.–C. Auger, B. Stout, Y. Pan, J. R. Bottiger, R. K. Chang, and G. Videen, "Observations and calculations of light–scattering from clusters of spheres," Appl. Opt. **39**, 6873–6887 (2000) and references therein.
2. P. Kaye, E. Hirst, and Z. Wang-Thomas, "A neural–network–based spatial light–scattering instrument for hazardous airborne fiber detection," Appl. Opt. **36**, 6149–6156 (1997).
3. D. D. Weis and G. E. Ewing, "Water content and morphology of sodium chloride aerosol particles," J. Geophys. Res. **104**, 21,275–21,285 (1999).
4. J. N. Seinfeld, S. N. Pandis, *Atmospheric chemistry and physics*, (John Wiley & Sons, New York, 1998), p. 514.
5. K. H. Leong, "Morphological control of particles generated from the evaporation of solution droplets: Theoretical considerations," J. Aerosol Sci., 511–524 (1987).
6. R. J. Cheng, D. C. Blanchard, and R. J. Cipriano, "The formation of hollow sea–salt particles from the evaporation of drops of seawater," Atmos. Res. **22**, 15–25 (1988).
7. U. K. Krieger and C. Braun, "Light–scattering intensity fluctuations in single aerosol particles during deliquescence," J. Quant. Spectrosc. Rad. Transf., in press.
8. D. R. Lide, *CRC Handbook of chemistry and physics*, 79th ed., (CRC Press, Boca Raton, 1998).
9. E. J. Davis and R. Periasamy, "Light–scattering and aerodynamic size measurements for homogeneous and inhomogeneous microspheres," Langmuir **1**, 373–379, (1985).
10. T. Koop, A. Kapilashrami, L. T. Molina, and M. J. Molina, "Phase transitions of sea–salt/water mixtures at low temperatures: Implications for ozone chemistry in the polar marine boundary layer," J. Geophys. Res. Atmos **105**, 26393–26402 (2000).
11. G. Videen, P. Pellegrino, D. Ngo, J. S. Videen, and R. G. Pinnick, "Light–scattering intensity fluctuations in microdroplets containing inclusions," Appl. Opt., **36**, 6115-6118 (1997).
12. J. Gu, T. E. Ruekgauer, J.–G. Xie, and R. Armstrong, "Effect of particulate seeding on microdroplet angular scattering," Opt. Lett. **18**, 1293–1295 (1993).

#30236 - $15.00 US Received January 17, 2001; Revised February 19, 2001

(C) 2001 OSA

13. Schäfer K, Lax E. *Eigenschaften der Materie in ihren Aggregatzuständen*, II2 Bestandteil b of Landolt-Börnstein Zahlenwerte und Funktionen in Physik, Chemie, Astronomie, Geophysik und Technik. (Springer, Berlin, 1962), pp. 3-25.
14. M. D. Cohen, R. C. Flagan, and J. H. Seinfeld, "Studies of concentrated electrolyte solutions using the electrodynamic balance. 3. Solute nucleation," J. Phys. Chem. **91**, 4583–4590 (1987).
15. W. K. Burton, N. Cabrera, and F. C. Frank, "The growth of crystals and the equilibrium structure of their surfaces," Phil. Trans. Roy. Soc. A **243**, 299–358 (1951).
16. H. R. Pruppacher, J. D. Klett, *Microphysics of clouds and precipitation*, 2nd rev. and enl. ed., (Kluwer Acadamic, Dordrecht, 1997), pp. 95.
17. ibid., p. 507.
18. W. C. Hinds, *Aerosol Technology*, 2nd ed., (John Wiley & Sons, New York, 1999), p. 296.
19. ibid., p. 287.

1 Introduction

The light–scattering properties of non–spherical aerosol particles are of interest for a number of reasons. Such aerosols have been found to play an important role in different fields, ranging from health sciences to industrial and environmental problems. For aerosol sphericity will affect the scattering albedo of atmospheric aerosol particles and hence will influence the radiation budget of the earth.

Measuring the two–dimensional angular optical scattering (TAOS) of such particles is of interest for testing computer codes calculating such scattering [1]. Taken a step further, TAOS may be used as an analytical tool. Hirst et al. showed that TAOS can be used for characterizing asbestos fibers [2]. Here we present a method of analyzing the two–dimensional scattering pattern to gain a better understanding of the internal morphology of composite particles. One example of such particles in an environmental context are sea–salt aerosol particles injected into the atmosphere by wave action on the Earth's oceans. Sea–salt aerosols are known to participate in a variety of heterogeneous reactions [3], with reaction rates strongly depending on the water content. Under atmospheric conditions sea–salt particles often contain a solid phase in equilibrium with an aqueous solution [4]. Obviously, it is of crucial importance whether the liquid phase is in contact with the gas phase or not. Therefore, there has been considerable discussion about the morphology of such particles, i. e. whether upon evaporation the particles form a solid shell shielding the remaining liquid from contact with the gas phase or a solid core exists with an aqueous solution shell around it [3, 5, 6].

Recently, we have shown that the measurement of temporal light–scattering intensity fluctuations of single aerosol particles can be used to deduce solid–to–liquid partitioning in ternary systems such as NaCl–$CaCl_2$–H_2O [7]. However, this method is ill–suited for resolving fast processes as the efflorescence of a micron sized NaCl crystal from a supersaturated aqueous solution. In the following we present a method to determine the solid–to–liquid partitioning by calculating a distortion parameter from TAOS patterns, which yields a faster time resolution. For calibrating this parameter we use the deliquescence of a single NaCl particle levitated in an electrodynamic balance: during deliquescence water is taken up from the gas phase and forms an aqueous solution shell around the particle. The size of the solid NaCl core will shrink continuously during deliquescence while the concentration of the aqueous solution will remain constant. The volume ratio of the solid and the surrounding liquid can be measured simultaneously with TAOS.

2 Experimental

The levitated aerosol droplet is stored in a double–ring electrodynamic balance as shown in Fig. 1. The balance is placed in a three wall glass chamber, with a cooling liquid flowing through the inner walls and an insulation vacuum between the outer walls. The

#30236 - $15.00 US Received January 17, 2001; Revised February 19, 2001
(C) 2001 OSA

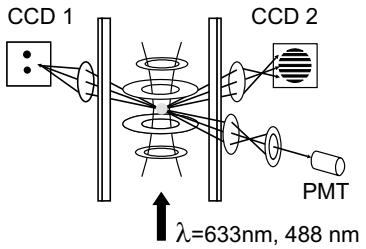

Fig. 1. Schematic plot of the electrodynamic balance employed for the aerosol droplet storage. Scattered laser light of two wavelengthes is monitored by two CCD–sensors, one in the optical near field for position information fed to the U_{DC}–feedback loop for the vertical stabilisation of the particle, the other in the optical far field for pattern distortion parameter and Mie scattering analysis. An additional photo multiplier tube is used to measure the temporal light–scattering fluctuations.

temperature inside the chamber was fixed at 263.5 K, with a stability of better than 100 mK and an accuracy of ±0.5 K. A constant gas flow (30 standard cubic centimeters per minute) of a N_2/H_2O–mixture with a controlled H_2O partial pressure is pumped continuously through the chamber at a constant total pressure of 330 mbar. The relative humidity (RH) inside the chamber can be varied by changing the N_2/H_2O–ratio using automatic mass flow controllers.

For the optical studies we use either a HeNe laser ($\lambda = 633$ nm) or an Ar^+ laser ($\lambda = 488$ nm) to illuminate the particle. Several methods are then employed to characterize the aerosol particle during an experiment. First, we use the near field video image of the particle on CCD 1 (JAI CV–M50, image sensor: Sony ICX038DLA, 768×494 pixel, 25 fps) and an automatic feedback loop to adjust the DC voltage (U) for compensating the gravitational force. Thus, a change in DC voltage is a direct measure of the mass change of the aerosol particle. In the NaCl/water–system the density of the solid and the density of the aqueous NaCl solution in equilibrium with the solid is well known [8], therefore this mass change data can be used to calculate an effective radius of the NaCl crystal within the host. Second, we compare the regular fringe pattern of the elastically scattered light on CCD 2 (JAI CV-M40, image sensor: Sony ICX074AL, 648×494 pixel, 60 fps, progressive scan, used in auto–gain mode, observed angles ranging from 78° to 101°) with Mie theory. If the particle is liquid, and therefore of spherical shape, the mean distance between the fringes can be used to calculate the radius of the particle, almost independent of its refractive index [9]. If a liquid–to–solid transition occurs, the fringe pattern looses its regular periodic structure and becomes totally irregular (see Fig. 2, right panel).

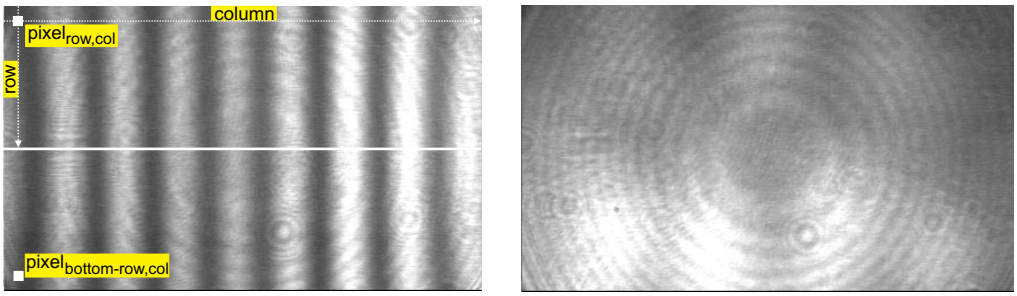

Fig. 2. Scheme for calculating the pattern distortion parameter from an individual 2D scattering pattern: liquid particle on left panel, solid particle on right panel. The concentric circles seen on both images are not an effect of the scattering of the particle but are due to scattering of the monochromatic light by the CCD's protective glass cover (thickness: 750 μm).

#30236 - $15.00 US
Received January 17, 2001; Revised February 19, 2001
(C) 2001 OSA

Third, we use a photomultiplier with a relatively small conical detection angle (approximately 0.2° half angle) to measure the scattering intensity. By feeding this signal to an analogue lock-in amplifier (Stanford Research System SR510) we measure the intensity fluctuations at the frequency of the AC field of the electrodynamic trap with a 10 Hz ENBW. Additionally, from the images of CCD 2 we also calculate a value for the asymmetry in the scattering pattern, which we term *pattern distortion parameter* Δ.

Fig. 2 shows how to calculate the pattern distortion parameter. The intensity of every single pixel in the images' upper half is compared to the colour value of the corresponding pixel in the lower half according to the following formula:

$$\Delta = \sum_{i}^{\text{row}} \sum_{j}^{\text{column}} (\text{pixel}_{ij} - \text{pixel}_{\text{bottom row}-i,j})^2 \Big/ (\text{row}/2 \cdot \text{column})^2$$

Obviously, Δ will be larger for non–symmetric images as shown in the right panel of Fig. 2.

3 Results

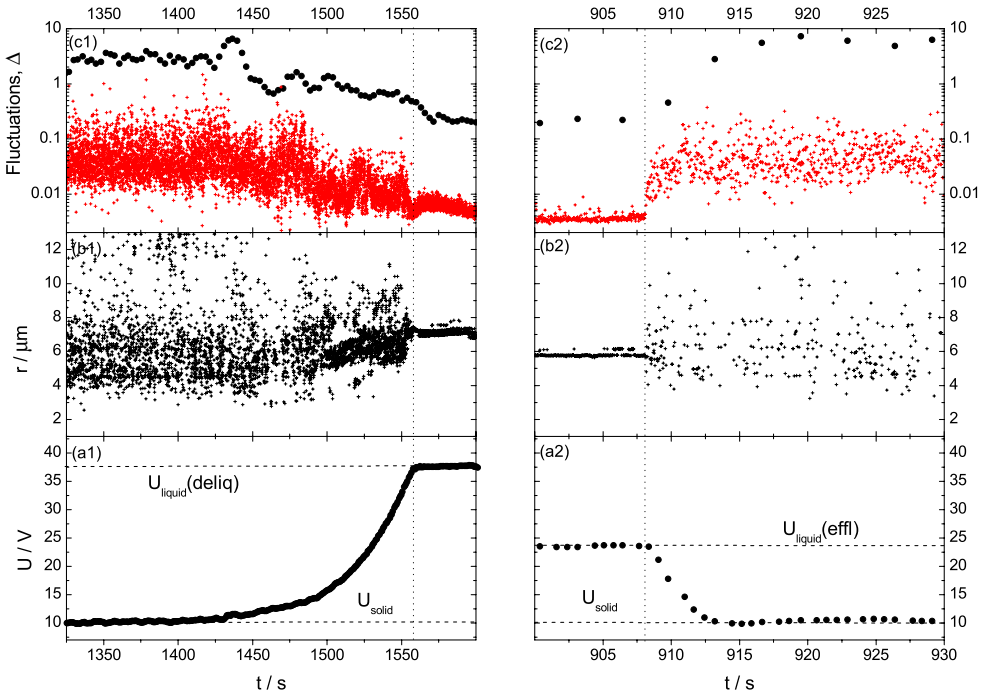

Fig. 3. Raw data of a deliquescence experiment (left) and an efflorescence experiment (right). For each experiment the DC voltage U compensating the gravitational force (panel a1 and a2), the radius r determined from the fringe pattern on CCD2 (panels b1 and b2), and the temporal fluctuation data (panels c1 and c2, full circles) and the pattern distortion parameter Δ (red crosses) are plotted versus time. Relative humidity in the deliquescence experiment: RH=75%±2%, RH is increasing with a nominal rate of $2.5 \cdot 10^{-3}$%/s. For the efflorescence experiment: RH=37%±2%. RH is decreasing with a nominal rate of $9 \cdot 10^{-3}$%/s. Note that the time scale is stretched by about a factor of 10 for the efflorescence experiment. As a guide to the eye, the vertical dotted lines indicate the end of the deliquescence process and the start of the efflorescence process, respectively.

We have performed about 50 deliquescence/efflorescence cycles with a micron sized NaCl particle. Figure 3 shows data sections of a typical deliquescence (left panel) and

#30236 - $15.00 US
Received January 17, 2001; Revised February 19, 2001
(C) 2001 OSA

a typical efflorescence (right panel). At elevated relative humidities inside the chamber ($RH \geq RH_{deliq} = 75\%$, left panel) water is taken up by the initially crystalline NaCl particle. Hence, its mass increases from the value for the solid particle (proportional to U_{solid}, see panel a1) until the constant value for the completely liquid particle is reached (proportional to $U_{liquid}(deliq)$). The radius measurement fails for the case of solid particles (no regular fringe pattern present resulting in a large scatter in the data) but yields constant values for the particle in the liquid state (panel b1). Note the decreasing scatter of the radius data with increasing water uptake. The uppermost panel (c1) shows the temporal fluctuation measurement and the measurement of the pattern distortion parameter on a logarithmic scale. Both values start to decrease just when the particle starts taking up water and reach a constant value when the particle is completely deliquesced. The noise level of the pattern distortion parameter Δ is higher than expected for pure pixel noise because misalignment and optical distortions caused by the optical elements (see Fig. 2) will contribute to it. The scatter in the temporal fluctuation data and in the pattern distortion parameter remains large as long as a solid inclusion is present. While the individual temporal fluctuation data are inherently averaged data (10 Hz ENBW), which means that the inclusion occupies different positions within the liquid host for each data point, the individual pattern distortion data are calculated from images taken with a shutter speed of 1/250 s and are therefore representative for a specific position of the inclusion in the host. Hence, the time resolution for the pattern distortion parameter is about a factor of 10^2 faster than that of the temporal fluctuation measurement.

The efflorescence (Fig. 3, right panel, $RH \approx RH_{effl} = 37\%$) is a much faster process, therefore the time scale applied to the panels is stretched by a factor of about 10. Furthermore, efflorescence will only occur in supersaturated solutions so that the particle — being in a metastable state [10] — has already lost a substantial amount of water: its initial mass ($U_{liquid}(effl)$) being only a mere two thirds of that of the deliquesced particle. Apparently, the radius of the particle just before the efflorescence has decreased notably as well. The fluctuation values and the pattern distortion parameter values should not be influenced by the decrease in radius since the particle is still completely liquid and of spherical shape. This holds true also for the temporal fluctuations, whereas the pattern distortion parameter data are decreased by a factor of about 1.5. Now optical distortions contribute less to the pure pixel noise since the number of fringes has decreased resulting in a lower noise level. When efflorescence occurs the mass data drop to the value of U_{solid}, the radius data scatter, the fluctuation values and the pattern distortion parameter data increase. The time to complete solidification takes about 2 seconds as can be seen from both the DC voltage data and the pattern distortion parameter data. Two points should be stressed: first, the DC voltage feedback is fast enough to follow the process. Otherwise, the DC voltage would lag behind the pattern distortion parameter data which are not influenced by an unbalanced DC voltage. Second, the temporal fluctuation measurement is not fast enough to resolve the efflorescence process.

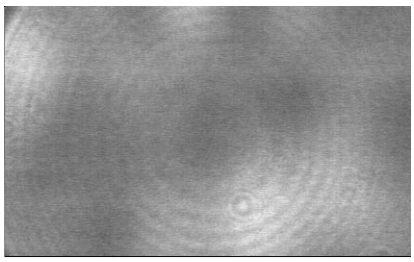

Fig. 4. (2.2 MB) Movie of the deliquescence.

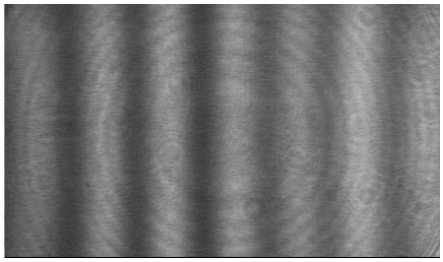

Fig. 5. (1.96 MB) Movie of the efflorescence.

#30236 - $15.00 US Received January 17, 2001; Revised February 19, 2001
(C) 2001 OSA

In figures 4 and 5 two movies produced from the images of CCD 2 are shown, one for the deliquescence process of Fig. 3 and one for the efflorescence process of Fig. 3. Both movies are shown in real–time: approx. 31 frames per second for the efflorescence movie but only 3 frames per second for the deliquescence movie due to the longer process. While during deliquescence a fringe pattern can be recognized even before the particle is completely liquid (pattern comes to a virtual standstill), after efflorescence the regular pattern vanishes almost instantly.

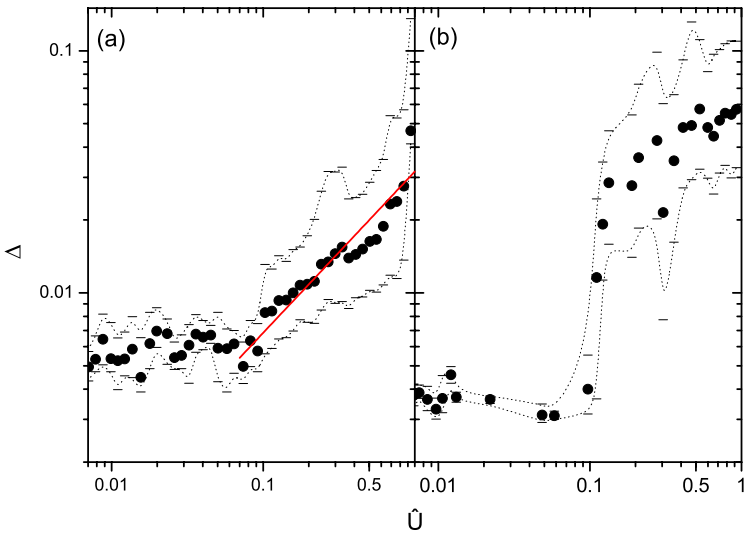

Fig. 6. Calculated median of Δ from 27 deliquescence (panel a) and 22 efflorescence processes (panel b) of the same particle as a function of $\hat{U}$. For deliquescence: $\hat{U} = (U - U_{\mathrm{liquid}}(\mathrm{deliq})/(U_{\mathrm{liquid}}(\mathrm{deliq}) - U_{\mathrm{solid}})$, and for efflorescence: $\hat{U} = (U_{\mathrm{liquid}}(\mathrm{effl}) - U)/(U_{\mathrm{liquid}}(\mathrm{effl}) - U_{\mathrm{solid}})$. U is the DC voltage to compensate for gravitational force, all other voltage values are constant and taken from Fig. 3. Error bands are between the second and the fourth quintile, red line see text.

Figure 6 shows the dependence of the pattern distortion parameter on the reduced mass change $\hat{U}$ (see caption of Fig. 6 for definition) for all analysed deliquescence and efflorescence processes. $\hat{U}$ is proportional to the solid–to–liquid mass partitioning of the particle during deliquescence [7]. Because of the noise level of Δ we cannot detect values of $\Delta \lesssim 0.006$, but for $\hat{U} \gtrsim 0.1$ we find a power law dependence proportional to $m^{2/3}$ (red line in Fig. 6), m being the mass of the solid inclusion, revealing that Δ is proportional to the area of the solid inclusion. For the temporal fluctuations such a dependence was suggested by modelling and earlier experimental work [11, 12, 7]. Therefore, we believe the pattern distortion parameter can be used as an analytical tool to measure solid–to–liquid partitioning in single aerosol particles.

For the efflorescence processes the reduced mass change dependence of the pattern distortion parameter shows a completely different behaviour: for values of $\hat{U} < 0.1$ the pattern distortion parameter is constant (but smaller than for the deliquescence, see discussion of Fig. 3) as is the case for the deliquescence but for values larger than 0.1 one sees a sharp increase levelling to the same value of Δ for the solid particle. This suggests that the morphology of the solid NaCl being formed by efflorescence in the aerosol droplet differs dramatically from the one present in the deliquescence process.

#30236 - $15.00 US
Received January 17, 2001; Revised February 19, 2001
(C) 2001 OSA

4 Discussion

As mentioned above, before efflorescence can occur the aqueous solution droplet becomes highly supersaturated with respect to the NaCl solid phase. Therefore, the crystal growth will proceed in two steps. During the first step, the liquid in contact with the growing crystal will dilute — due to losing NaCl to the crystalline phase — until it reaches its thermodynamic equilibrium composition. This step does not require any mass interchange with the gas phase and hence, cannot be detected by the DC voltage feedback. The concentration of the aqueous solution increases from 26 wt.-% at the thermodynamic deliquescence point [13] to 41 wt.-% before the particle effloresces, see data of Fig. 3. Thus, roughly 36% of the supersaturated solution droplet mass will crystallize. This allows rescaling of Fig. 6 to absolute solid–to–liquid mass partitioning as shown in Fig. 7.

In a second step the particle will evaporate the remaining water of its liquid phase to the gas phase until it is completely crystallized. In the representation of Fig. 7 the difference between deliquescence and efflorescence is even more pronounced. Obviously the observed efflorescence cannot be described by a time reversed deliquescence process, i. e. growing a compact solid core in the liquid.

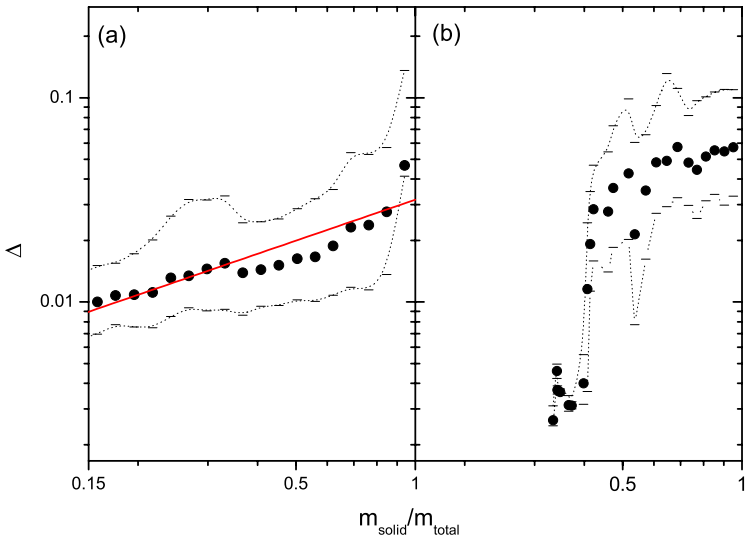

Fig. 7. Median of Δ as a function of solid–to–liquid mass partitioning. Left panel for the deliquescence, right panel for efflorescence. Error bands are between the second and the fourth quintile.

Instead of growing a compact solid one could imagine dendritic growth of the solid. This may qualitatively describe the steep increase of Δ in panel b of Fig. 7. However, we can easily detect a compact solid core of solid–to–liquid mass partitioning of $m_{\mathrm{solid}}/m_{\mathrm{total}} > 0.15$ as seen in panel a of Fig. 7. But as Δ does not increase above the noise level for $m_{\mathrm{solid}}/m_{\mathrm{total}} < 0.4$ for the efflorescence process dendritic growth is rather unlikely.

In our opinion the most likely mechanism is growing a solid shell around the liquid which collapses at $m_{\mathrm{solid}}/m_{\mathrm{total}} \approx 0.4$ due to mechanical stress. For $m_{\mathrm{solid}}/m_{\mathrm{total}} < 0.4$ the particle keeps its spherical symmetry with Δ–values at the noise level, but after collapsing the then irregularly shaped particle shows Δ–values similar to those found for a completely solid NaCl particle. This is supported not only by other experiments [6, 3]

#30236 - $15.00 US
Received January 17, 2001; Revised February 19, 2001
(C) 2001 OSA

and theoretical considerations [5] but also when estimating the duration of the efflorescence process as follows.

The inverse of the crystal growth rate [15] in highly supersaturated aqueous NaCl solution droplets at a temperature of -10°C can be estimated by:

$$\tau_1 = \frac{r_{\text{solid}}^2}{2\,S\,D_{\text{liquid}}}\,,$$

where r_{solid} is the radius of the solid particle after efflorescence, S the dimensionless supersaturation of the aqueous solution with respect to the solid, and D_{liquid} the liquid diffusion constant. Taking $D = 1.7 \cdot 10^{-6}$ cm^2/s (extrapolated from its value at 298 K [8] to $-10\,^{\circ}$C by using the temperature dependence for pure water [16]), $r_{\text{solid}} = 2.8$ μm (using the data of Fig. 3), and $S = 400\%$ [14] this leads to a time $\tau_1 = 6 \cdot 10^{-3}$ s.

The time for evaporation of the water to the gas phase is limited by gas phase diffusion and given by [18]:

$$\tau_2 = \frac{R\,\varrho\,(4r_{\text{liquid}}^2 - 4r_{\text{solid}}^2)}{8 D_{\text{gas}} M \left(\frac{p_d}{T_d} - \frac{p_\infty}{T_\infty}\right)}\,,$$

here R is the gas constant, ϱ the density of the particle, r_{liquid} the radius of the droplet before efflorescence, r_{solid} the radius of the solid particle after efflorescence, D_{gas} the gas phase diffusion constant, M the molar mass of water, p_d is the partial pressure of water vapour at the droplet surface, T_d is the droplet temperature, p_∞ is the partial pressure of the water in the chamber, and T_∞ the temperature in the chamber. Taking $D_{\text{gas}} = 0.1$ cm^2/s [17], estimating T_d from the supersaturation of the water vapour pressure at the droplet surface with respect to the water vapour pressure in the chamber [19], and using the data from Fig. 3 we calculate a duration of $\tau_2 = 4 \cdot 10^{-4}$ s for the evaporation[1]. The estimated total time for efflorescence will be less than 10 ms. However, the observed duration of about 2 seconds is indicating a diffusion barrier. A solid shell surrounding the liquid could provide such a barrier.

While the experimental data in combination with the calculations presented above indicate the formation of a solid shell during efflorescence further experiments are needed to prove this possible crystallization mechanism.

Acknowledgements

We would like to thank Thomas Peter, Beiping Luo, and Thomas Koop for many helpful discussions.

[1]NB during deliquescence supersaturation is minimal so that $p_d/T_d - p_\infty/T_\infty$ approaches zero, which in turn leads to a much larger τ_{deliq}.

#30236 - $15.00 US Received January 17, 2001; Revised February 19, 2001
(C) 2001 OSA